北見工業大学研究報告
第17巻 第1号 (昭和60年)

Memoirs of the Kitami Institute of Technology
Vol. 17 No. 1 (1985)

LDV Measurements in Two-Dimensional Bent-over Jets (Part I)*

—Mean flow properties and curvature effects on turbulence structures of nonbuoyant jets—

by Hiroyuki HANIU**

(Received April 12, 1985)

Abstract

An experimental study of two-dimensional bent-over nonbuoyant jets which are characterized by streamline curvature is reported. The experimental data include mean and turbulent flow properties obtained from measurement of instantaneous velocity and temperature in the flow. The experiments were conducted in a hydroulic flume using Laser Doppler Velocimetry (LDV) and resistance thermometry. The mean flow properties studied are trajectories of the jets, mexing rate, velocity and temperature distributions. In the turbulent flow studies, the effects of streamline curvature on turbulence structure were investigated. There, turbulence intensities, Reynolds stress, intermittency and turbulent spectra are calculated. The measurements extended over the near-to-intermediate field, namely $y/D<60$, where y is the distance along the flume and D is the width of the jet at the exit. In spite of the presence of strong streamline curvature, streamwise mean velocity distributions are found to be nearly Gaussian when scaled properly. The trajectory of the maximum velocity point scales with length scale based on the kinematic momentum flux and follows a half power law. Even if the buoyancy effects are absent, it is rather difficult to isolate the curvature effects from the combined effects of curvature and nonequilibrium in the outer portion of the curved jets. However, the stabilizing effects of curvature in the inner portion and the destabilizing effects in the outer portion can be clearly seen from an isotropy parameter of the turbulent fluctuations and the temperature fluctuations.

1. Introduction

Experiments were performed on two-dimensional jets of water discharged vertically into a cross-flowing ambient in a hydraulic flume. Such flows are encountered in many practical situations, such as discharged air from cooling towers, smoke-stack exhaust, thermal discharges to rivers, vents of liquified natural gas carriers, etc. These flows are often buoyancy-driven. However, in this study cases are limited to slightly heated jets, which show no significant buoyancy effects but yield sufficient temperature information so as to isolate the curvature effects from buoyancy. The temperature information without significant density differences will give alternative information for the diffusion process of polluted material discharged into the Environment.

* Part of this report was prosented at the ASCE Forth Engineering Mechanics Division Specialty conference (Purdue University U. S. A. May 1983).

** Department of Mechanical Engineering, Kitami Institute of technology.

When a jet is discharged into a crossflowing ambient, the trajectory of the jet is bent due to the mixing of the momentum of the two fluids and is swept downstream. As a result the flow is characterized by streamline curvature and flow recirculation downsteram, behind the jet.

In the buoyancy-driven flows it is well known that the gradient Ricahrdson number[10] defined as

$$Ri_g = \frac{g(\partial T/\partial x)}{T(\partial U/\partial x)^2} \tag{1}$$

where g is the gravitational acceleration characterizes buoyancy effects on various turbulent quantities. In the flows with streamline curvature, from the concept of analogy between streamline curvature and buoyancy[4] one can derive the equivalent curvature Ricahrdson numbers, which can characterize curvature effects. It is now known that the effects of curvature are such as to increase the turbulent shear-stress in a shear layer, when the quantity

$$\frac{U}{(R+n)(\partial U/\partial n)} \tag{2}$$

is negative, where U is mean velocity along the streamline, R is radius of curvature and n is the coordinate directed normal to the streamline and directed away from the center of curvature. In such a case the curvature is said to be destabilizing and in the opposit case, it is said to be stabilizing. It can easily be seen that in the case of bent-over jets, the outer portion of the jet is destabilized while the inner portion is stabilized.

In order to focus on the details of the turbulent structure, it is descirable to keep the flow configuration as simple as possible. Hence two-dimensional flows with mild recirculation behind the jet were selected. The jet in crossflow provides an excellent opportunity to study in one flow both the stabilizing (in the inner portion) and destabilizing (in the outer portion) effects of curvature.

2. Experimental Procedure

The experiments were carried out in a hydraulic flume, 7.0 m long × 0.45 m wide × 0.75 m deep with 4.8 : 1 contraction. The side walls were made of 1.9 cm thick glass covering the first 2.4 m length for Laser beam passage. The rms intensity of the free stream turbulence u' without presence of the jet was found to be typically about 1% at a free stream velocity of 20 cm/sec, and spectral analysis showed vertually no fluctuations of very low frequencies. The jets emerged vertically into the crossflowing ambient through a 5 mm wide and 250 mm long slot nozzle, with an 8 : 1 turning contraction after cold and hot water were mixed at a desired temperature difference from ambient. The slot nozzle was located on the bottom floor, 1.8 m downstream of the flume entrance. The bottom floor near the nozzle was elevated 10 cm above the upstream floor, from 30 cm upstream of the nozzle, to the downstream, in order to prevent a boundary layer from developing along the bottom floor. The jet's development was confined

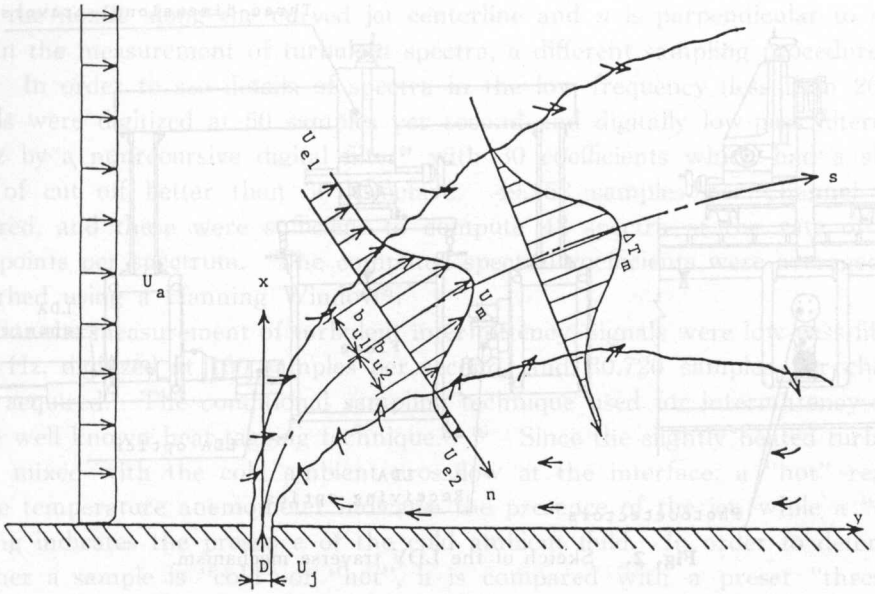

Fig. 1. Nomenclature and schematic view of the bent-over jet.

between two false vertical side walls of plexiglass 250 mm apart. The side walls were 1.4 m long and extended from 0.8 m upstream of the slot to 0.6 m downstream of the solt. Fig. 1 shows a schematic diagram of the flow configuration. The nominal mean jet velocity U_j at the slot exit was calculated from the discharge rate Q (measured using an orifice meter) and the area of the slot A. Thus, $U_j=Q/A$.

A two-channel Laser Doppler Velocimetry (LDV) with a 15 mw helium-neon Laser was used for instantaneous velocity measurements. The entire LDV system was mounted on an orthogonal three dimensional traverse, and a sketch of the traverse is shown in Fig. 2. The LDV was used in the 3-beam mode with a polarization technique in order to separate the two velocity components. Also, in order to measure the reversal of the flow direction, an Acousto-Optic Cell frequency shifter was used. The details of the arrangement of the various optical components are shown in Fig. 3. Velocity signals from the photo-detective devices are in the form of frequency. Two trackers were used to convert frequency signals into voltage signals, which were then digitized after low-pass filtering at 50 Hz. Since the frequency of turbulent eddies in the present study was mostly confined to below 10 Hz, this filter setting was high enough to cover all the important eddy frequencies.

Two quartz-coated fiber film probes 70 μm in diameter were combined with a Wheatston-bridge-type circuit with a constant current for instantaneous temperature measurements. One of the probes was placed approximately 1 mm downstream of the LDV focus point along the approximate streamline of the flow field. The other probe was placed in the crossflowing ambient, sufficiently upstream of the jet. A differential change of resistance is produced by the tem-

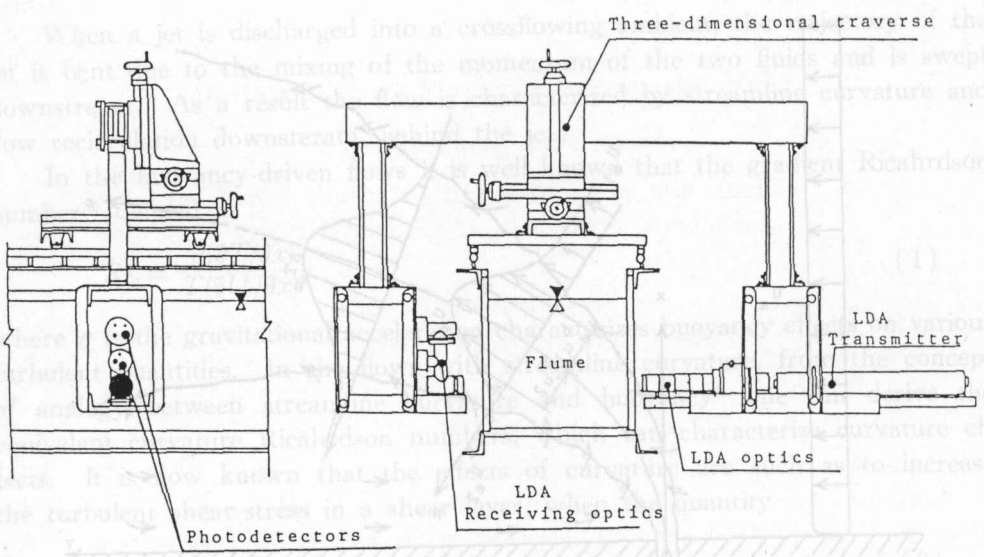

Fig. 2. Sketch of the LDV traverse mechanism.

1	:	Transmitter	8	:	Focusing lens
2 a, b, c, d	:	Polarization rotator	9	:	Objective lens
3 a, b	:	Beam splitters	10	:	Focusing secondary lens
4 a, b	:	Frequency shifter	11	:	Diagonal mirror
5	:	Centering prism	12	:	Beam splitter
6	:	Phase-shift compensator	13 a, b	:	Polarizers
7 a, b	:	Steering modules	14 a, b	:	Photodetectors

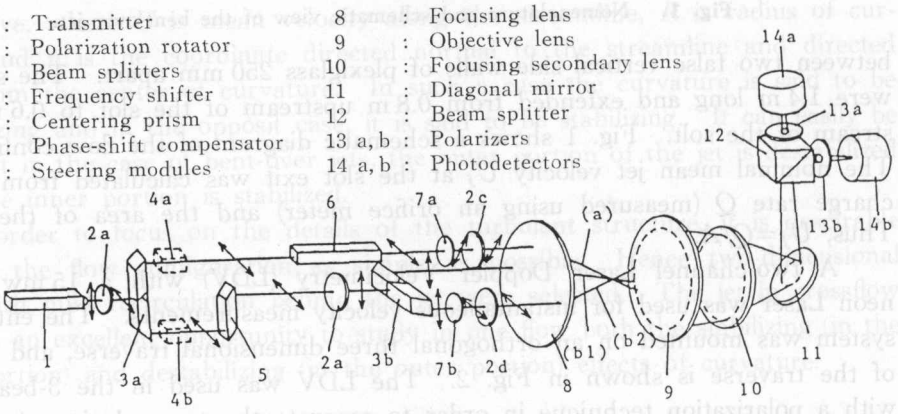

Fig. 3. Optical configuration of the 3-beam LDV.

prature difference and hence a differential voltage is produced across the bridge. This voltage across the bridge was amplified, low-pass filtered at 50 Hz and digitized together with the LDV signals. Sensitivity of the probe to velocity was checked, in cold water, by varying the velocity past the probe. There was no measurable sensitivity to velocity.

The low-pass filtered signals were sampled simultaneously at the rate of 20 samples per second, and a total of 2,560 samples per channel were obtained. Calculated quantities are the mean velocity U, V, mean excess temperature ΔT, and turbulence properties u', v', t', $\overline{uv}$, $\overline{ut}$, $\overline{vt}$, etc. These were first obtained in the flume coordinates, x (vertical) $-$ y (horizontal). Then the position of maximum velocity and the direction of the tangent to the jet centerline were obtained graphically from the mean flow data. All the calculated results in $x-y$ coordinates were then transformed into the jet coordinates, $s-n$, where s is measured

from the nozzle along the curved jet centerline and n is parpendicular to s.

In the measurement of turbulent spectra, a different sampling procedure was used. In order to see details of spectra in the low frequency (less than 20 Hz), signals were digitized at 50 samples per second and digitally low-pass filtered at 18 Hz by a nonrecursive digital filter[2] with 30 coefficients which had a sharpness of cut off better than 30 dB/octave. 49,152 samples per channel were acquired, and these were sufficient to compute 48 spectra at the rate of 1024 data points per spectrum. The computed spectral coefficients were averaged and smoothed using a Hanning Window[2].

For the measurement of turbulent intermittency, signals were low-pass filtered at 50 Hz, digitized at 100 samples per second, and 30,720 samples per channel were acquired. The conditional sampling technique used for intermittency study is the well known heat tagging technique.[1,7,11] Since the slightly heated turbulent jet is mixed with the cold ambient crossflow at the interface, a "hot" reading of the temperature anemometer indicates the presence of the jet, while a "cold" reading indicates the presence of the cold ambient fluid. In order to determine whether a sample is "cold" or "hot", it is compared with a preset "threshold level". If the sampled temperature is larger than the threshold level the sample and the velocity data taken at the same time are treated as "hot" samples, otherwise as "cold" samples. The accumlated number of hot samples divided by the total number of samples is defined as the intermittency γ. In order to eliminate subjectivity in determination of the threshold level, the threshold level was varied at equal intervals and intermittency was calculated for each thershold level. The intermittency decreases monotonically as the threshold level increases, but a plateau can be found where the variation of intermittency with threshold

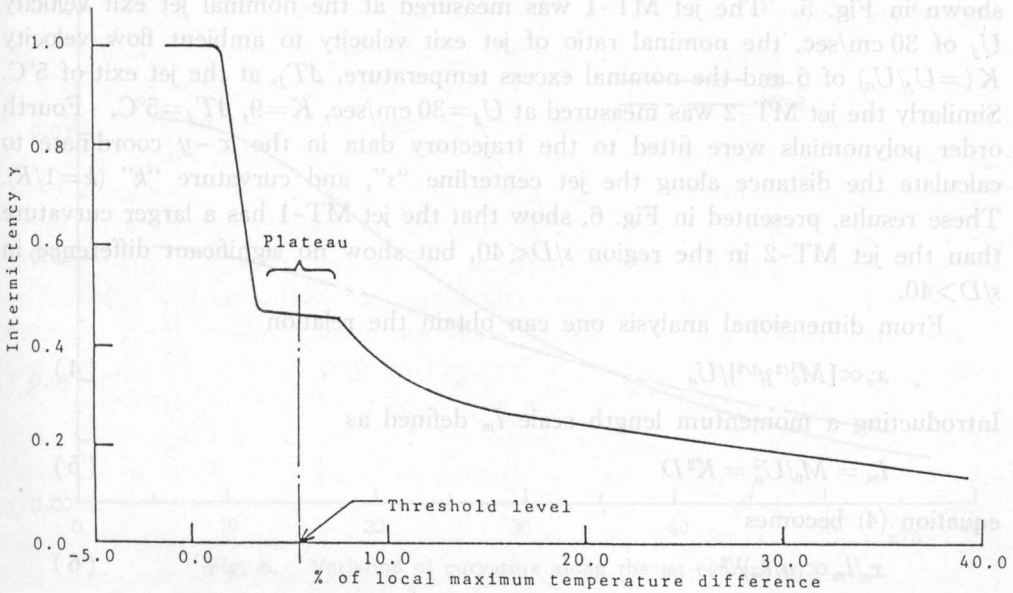

Fig. 4. Illustration of the determination of threshold level.

level is almost negligible. An illustration of the principle of determining the appropriate threshold level from the plot of intermittency against threshold level is given in Fig. 4. After the threshold level was determined from the recorded data, the same data were used to calculate intermittency and crossing frequency. The crossing frequency is defined as the number of zero crossings from hot to cold, divided by the averaging time.

A nominal jet exit velocity of 30 cm/sec was used and ambient crossflow velocities of 3.3 cm/sec and 5 cm/sec were chosen for the experiments. A nominal exit temperature difference of 5 deg.C was selected. At higher crossflow velocities, the jet bends too quickly and the two-dimensionality of the flow can not be maintained.

Before starting the LDV measurement, flow visualization was performed using dye injection to determine the approximate centerline of the jet. Then several cross-section were chosen approximately perpendicular to the centerline. The location for measurements at each cross-section were then decided.

3. Mean Flow Properties and Discussion

3-1. Trajectories

The vertical distance x_c of the trajectory (of the maximum velocity points) above the source plane at a distance y downstream from the source will be a function of crossflow velocity U_a, the initial momentum flux M_0 and the initial mass flux Q_0. Such that by defining $M_0=U_j^2 D$ and $Q_0=U_j D$,

$$f(x_c, y, U_a, M_0, Q_0)=0 \tag{3}$$

Trajectories of the maximum velocity points of two jets, MT-1 and MT-2, are shown in Fig. 5. The jet MT-1 was measured at the nominal jet exit velocity U_j of 30 cm/sec, the nominal ratio of jet exit velocity to ambient flow velocity $K(=U_j/U_a)$ of 6 and the nominal excess temperature, ΔT_j, at the jet exit of 5°C. Similarly the jet MT-2 was measured at $U_j=30$ cm/sec, $K=9$, $\Delta T_j=5$°C. Fourth order polynomials were fitted to the trajectory data in the $x-y$ coordinate to calculate the distance along the jet centerline "s", and curvature "k" ($k=1/R$). These results, presented in Fig. 6, show that the jet MT-1 has a larger curvature than the jet MT-2 in the region $s/D<40$, but show no significant difference in $s/D>40$.

From dimensional analysis one can obtain the relation

$$x_c \propto [M_0^{1/2} y^{1/2}]/U_a \tag{4}$$

Introducting a momentum length scale l_m defined as

$$l_m = M_0/U_a^2 = K^2 D \tag{5}$$

equation (4) becomes

$$x_c/l_m \propto (y/l_m)^{1/2} \tag{6}$$

As shown in Fig. 7, the experimental results of the two jets (with the exception

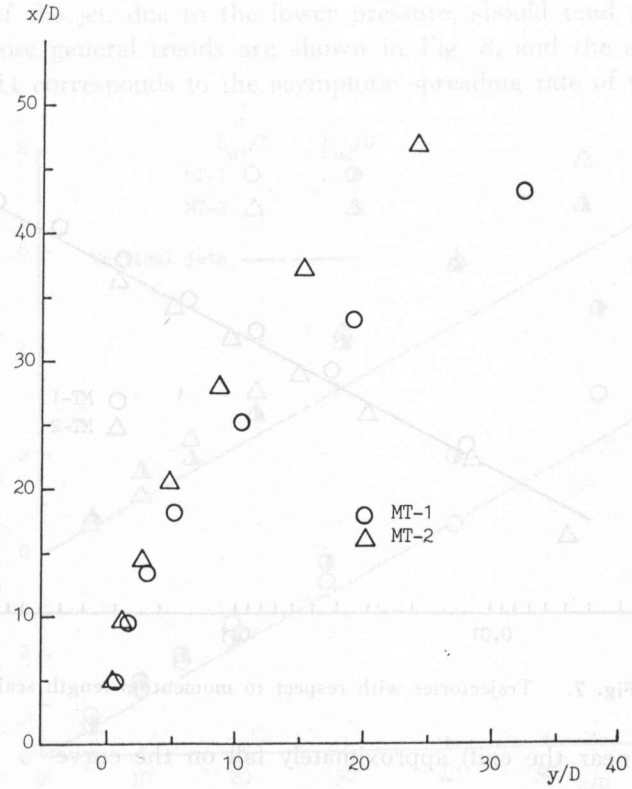

Fig. 5. Trajectories of jets.

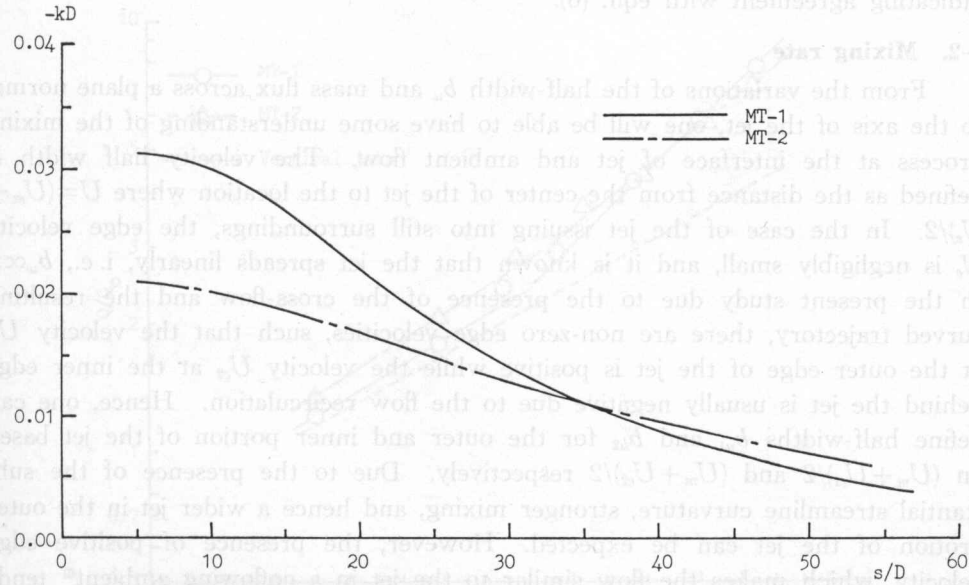

Fig. 6. Variation of curvature along the jet centerline.

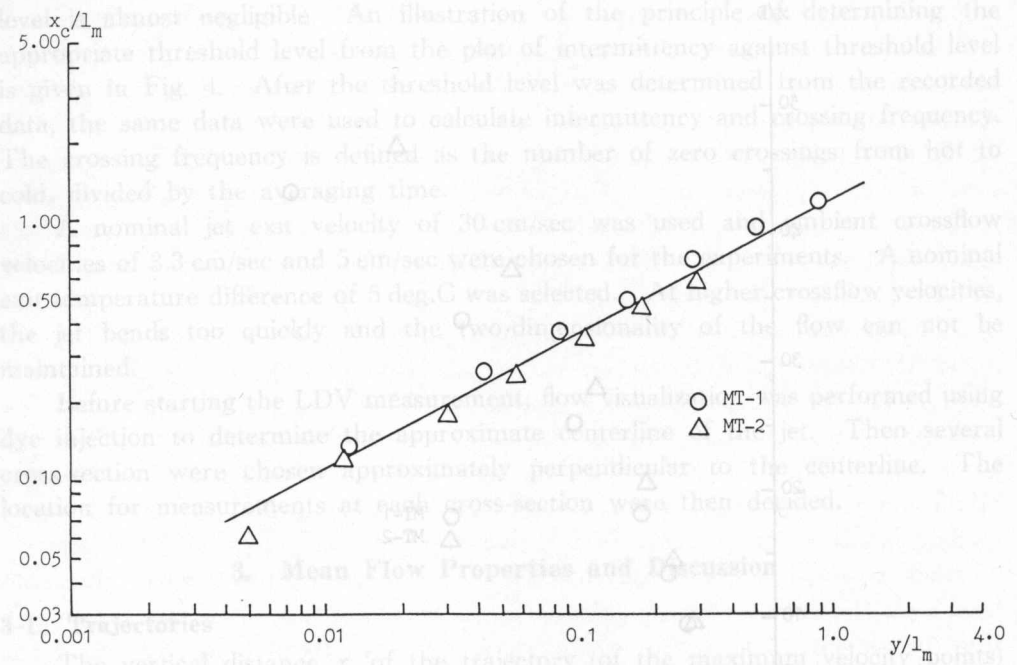

Fig. 7. Trajectories with respect to momentum length scale.

of those very near the exit) approximately fall on the curve

$$x_c/l_m = 1.2(y/l_m)^{0.51} \qquad (7)$$

indicating agreement with eqn. (6).

3-2. Mixing rate

From the variations of the half-width b_u and mass flux across a plane normal to the axis of the jet, one will be able to have some understanding of the mixing process at the interface of jet and ambient flow. The velocity half width is defined as the distance from the center of the jet to the location where $U=(U_m+U_e)/2$. In the case of the jet issuing into still surroundings, the edge velocity U_e is negligibly small, and it is known that the jet spreads linearly, i. e., $b_u \propto s$. In the present study due to the presence of the cross-flow and the resulting curved trajectory, there are non-zero edge velocities, such that the velocity U_{e1} at the outer edge of the jet is positive while the velocity U_{e2} at the inner edge behind the jet is usually negative due to the flow recirculation. Hence, one can define half-widths b_{u1} and b_{u2} for the outer and inner portion of the jet based on $(U_m+U_{e1})/2$ and $(U_m+U_{e2})/2$ respectively. Due to the presence of the substantial streamline curvature, stronger mixing, and hence a wider jet in the outer protion of the jet can be expected. However, the presence of positive edge velocity, which makes the flow similar to the jet in a coflowing ambient[6] tends to reduce the spread of the outer portion. Hence the effects of curvature and coflowing ambient counteract each other. The presence of recirculation on the

inner portion of the jet, due to the lower pressure, should tend to increase the spreading. Those general trends are shown in Fig. 8, and the straight broken line of slope 0.11 corresponds to the asymptotic spreading rate of vertical isother-

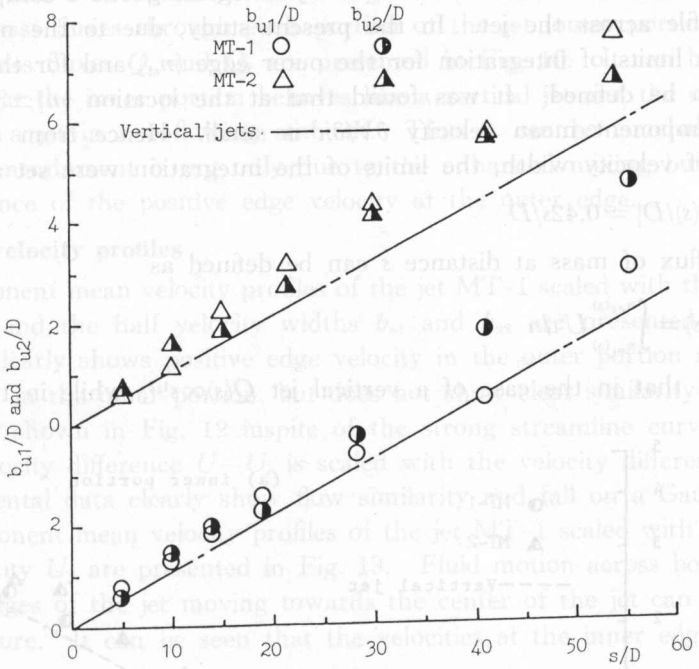

Fig. 8. Velocity half width along the jets.

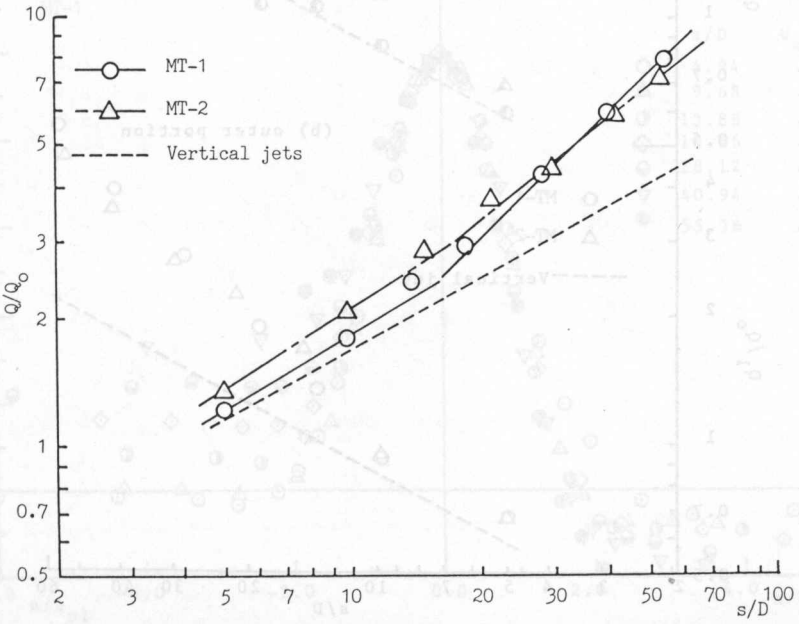

Fig. 9. Variation of the kinematic mass flux along the jets.

mal jets. The jet MT-1, with the strongest initial curvature, shows a higher spreading rate for the inner portion than the jet MT-2 due to the presence of stronger recirculation behind it.

The flux of mass can be obtained by integrating the s-component mean velocity profile across the jet. In the present study, due to the non-zero edge velocity, the limits of integration for the outer edge (n_{e1}) and for the inner edge (n_{e2}) have to be defined. It was found that at the location $|n| \simeq 3b_u$, variation of the n-component mean velocity $\partial V/\partial n$ is small. Hence from the averaged value of half velocity width, the limits of the integration were set as

$$|n_e(s)/D| = 0.42s/D \tag{8}$$

Hence the flux of mass at distance s can be defined as

$$Q(s) = \int_{n_{e1}(s)}^{n_{e2}(s)} U\, dn \tag{9}$$

It is known that in the case of a vertical jet $Q(s) \propto s^{1/2}$, while in the case of a

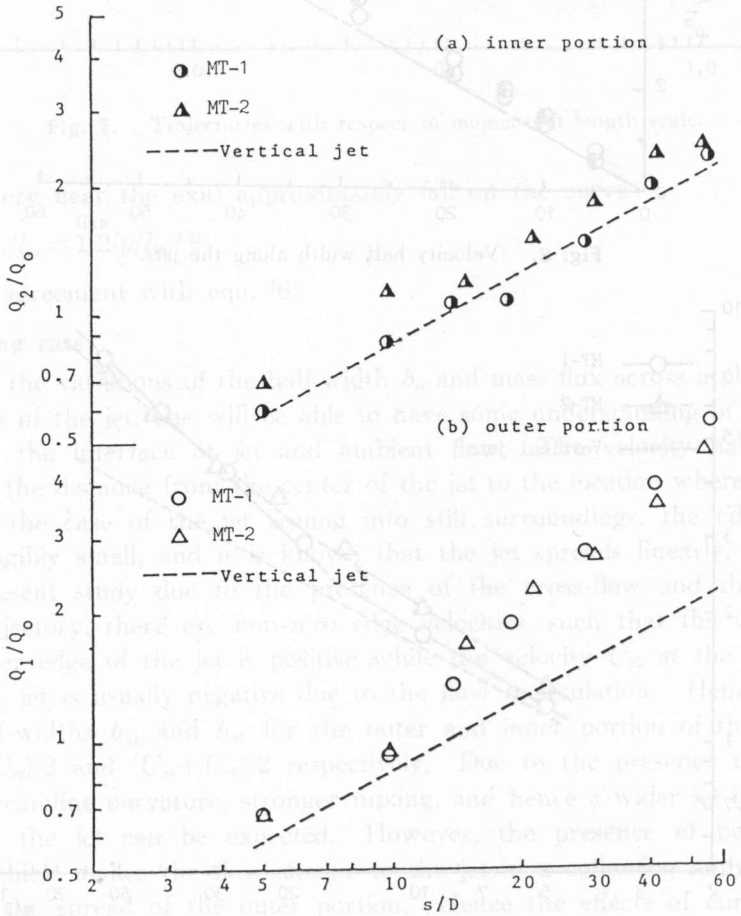

Fig. 10. Variation of the kinematic mass flux in each side of the jets.

jet in coflowing ambient $Q(s) \propto s$. Hence the jets in the present study can be expected to behave somewhat in between these two flows. Results presented in Fig. 9 show that both the jets tend toward the half-power relation at a small value of s/D and a linear relation at a larger value of s/D. It is also interesting to see the mass fluxes through each portion of the jet (outer portion and inner portion). Mass fluxes Q_1 and Q_2 are presented in Fig. 10. It can be seen from the figure that the inner portion behaves like a vertical jet and the outer portion behaves like a jet in a coflowing ambient. Thus it can be concluded that the increase of entrainment is not only due to the enhanced mixing but is also due to the presence of the positive edge velocity at the outer edge.

3-3. Mean velocity profiles

s-Component mean velocity profiles of the jet MT-1 scaled with the maximum velocity U_m and the half velocity widths b_{u1} and b_{u2} are presented in Fig. 11. The figure clearly shows positive edge velocity in the outer portion and negative edge velocity in the inner portion, but does not show clear similarity of the flow. However, as shown in Fig. 12 inspite of the strong streamline curvature, when the local velocity difference $U-U_e$ is scaled with the velocity difference U_m-U_e, the experimental data clearly show flow similarity and fall on a Gaussian curve.

n-Component mean velocity profiles of the jet MT-1 scaled with the nominal jet exit velocity U_j are presented in Fig. 13. Fluid motion across both the inner and outer edges of the jet moving towards the center of the jet can be observed from the figure. It can be seen that the velocities at the inner edge are nearly

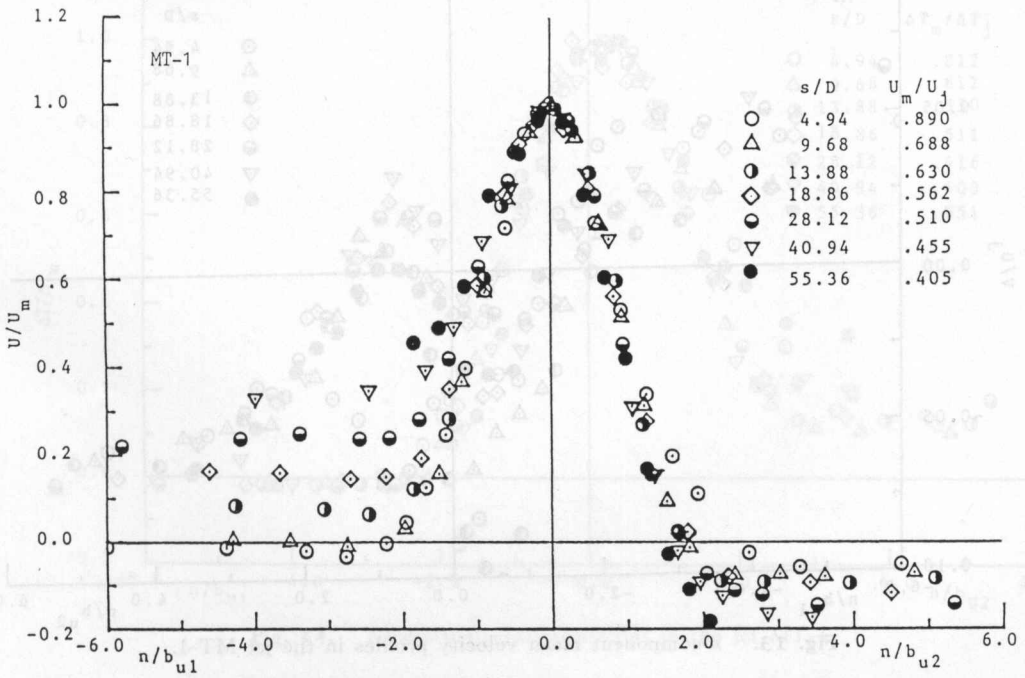

Fig. 11. s-component mean velocity profiles in the jet MT-1.

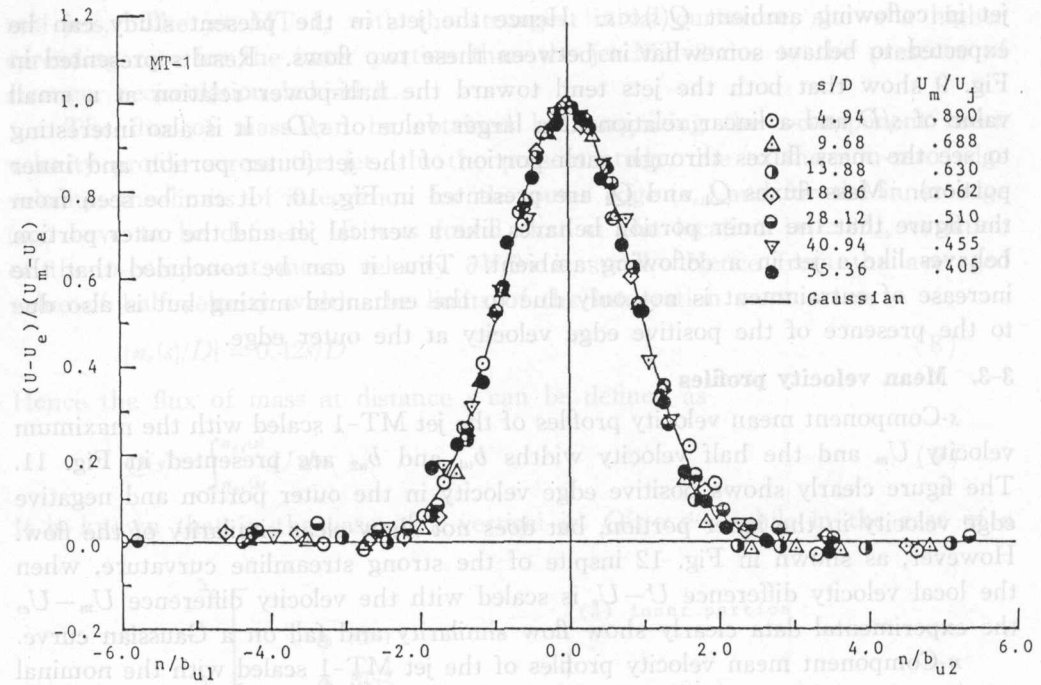

Fig. 12. s-component mean defect velocity profiles in the jet MT-1.

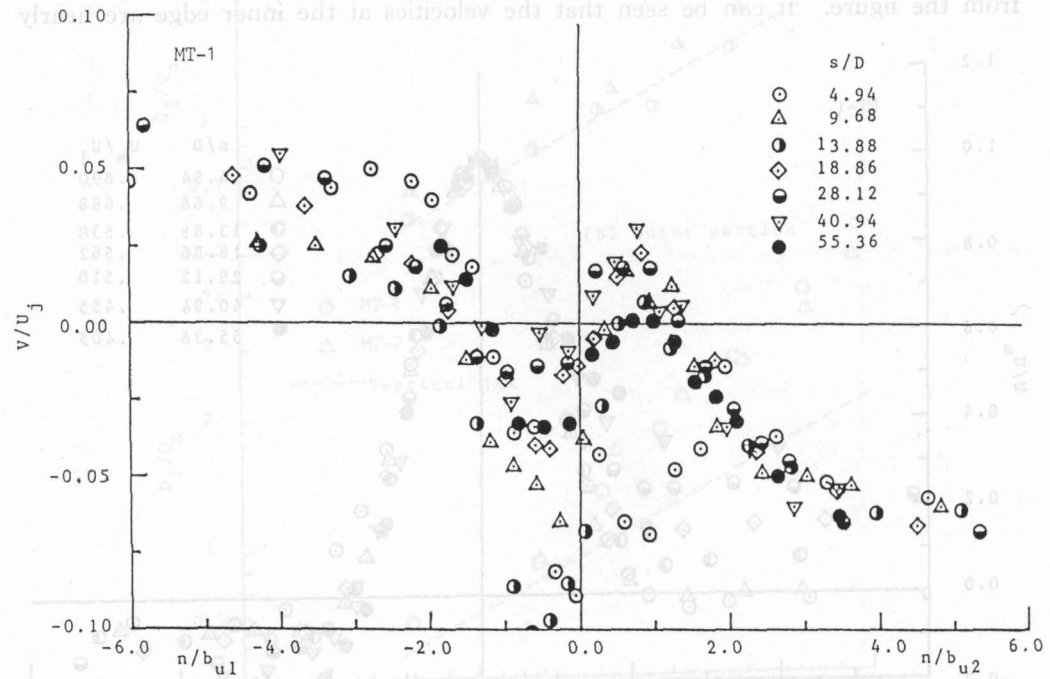

Fig. 13. n-component mean velocity profiles in the jet MT-1.

constant along the jet. This is due to the fact that recirculation determines these velocities rather than the jet turbulence. It is also very interesting to note that the n-component velocities at the center of the jet are negative at all the cross sections presented in the figure. This indicates that the fluid is moving from the inner portion to the outer portion of the jet. Due to the rapid increase of the flow rate in the outer portion, much more fluid needed to be entrained. Hence flow is entrained not only across the outer edge but also across the centerline. Similar results were obtained from the jet MT-2, but less dramatically due to its smaller streamline curvature.

3-4. Mean excess temperature profiles

Mean excess temperature profiles of the jet MT-1 are presented in Fig. 14. As one can see from the figure, substantial excess temperature can be observed beyond the inner edge of the jet, which is a result of the recirculation behind the jet. Also the excess temperature ΔT_{e2} at the inner edge was found to remain nearly constant at all s/D, rather than scaled with the local maximum excess temperature ΔT_m. This result is similar to that observed with edge velocities. It is also interesting to note that the locations of the maximum excess temperatures for all the profiles are shifted towards the inner portion from the centerline, i. e., the trajectories of the maximum excess temperature points lie below the respective velocity maximum trajectories.

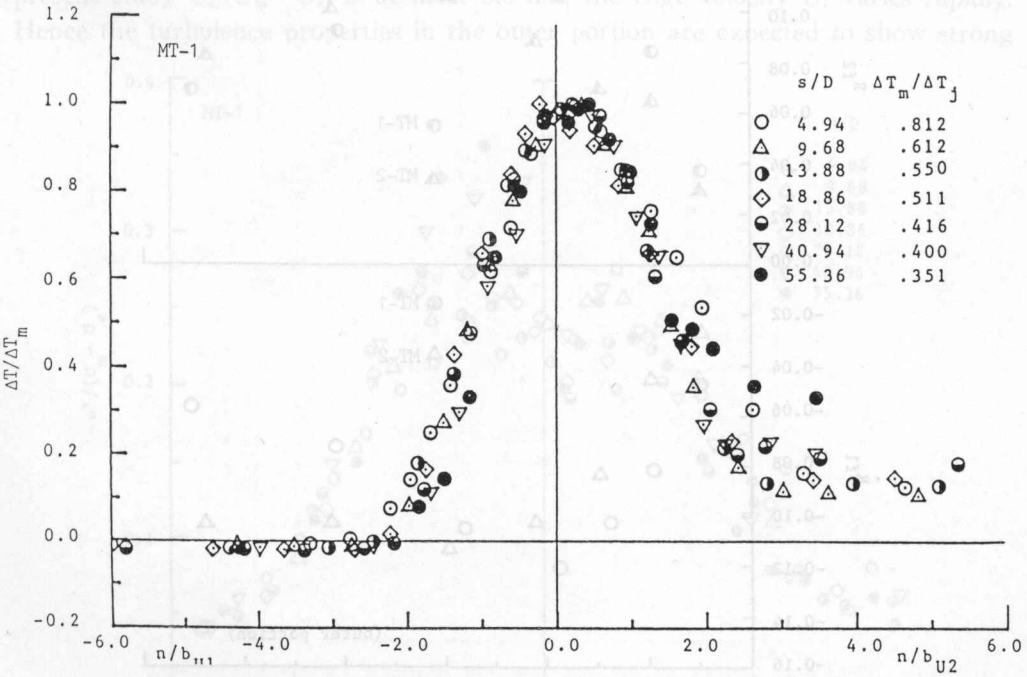

Fig. 14. Excess temperature profiles in the jet MT-1.

4. Turbulence Properties and Discussion

4-1. Curvature parameter

From analogy between streamline curvature and buoyancy[4] it was found that the flux Richardson number, R_f, defined as

$$R_f = \frac{2(U/r)}{\partial U/\partial n + U/r} \tag{10}$$

where $r=R+n$ (both r and R are negative in the present study) characterizes curvature effects on turbulence. This quantity is locally defined, hence it is convenient to define a global curvature parameter for each portion of the jet. Since it was found that the characteristic thickness of the shear layer is much smaller than the radius of curvature, the term $\partial U/\partial n + U/r$ can be approximated to $\partial U/\partial n$, hence

$$\hat{R}_f \simeq \frac{2(U/r)}{\partial U/\partial n} \tag{11}$$

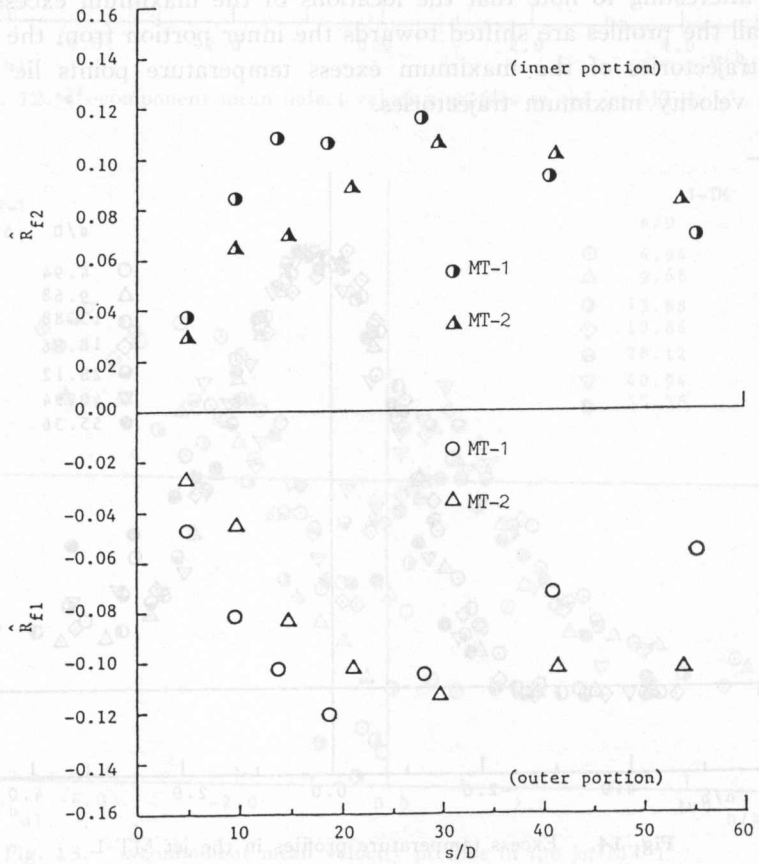

Fig. 15. Variation of global curvature flux Richardson numbers along the jets.

Using mean values of U and r for each portion, $U/r \simeq U_m/2R$ and $\partial U/\partial n \simeq U_m/2b_{u1}$ for the outer portion and $\partial U/\partial n \simeq -U_m/2b_{u2}$ for the inner portion. Thus the global curvature Richardson numbers can be expressed as

$$\hat{R}_{f1} \simeq 2b_{u1}/R \tag{12}$$

$$\hat{R}_{f2} \simeq -2b_{u2}/R \tag{13}$$

Variation of the global curvature Richardson number along the jets MT-1 and MT-2 is presented in Fig. 15. As one can see from the figure, the values of the curvature parameter are approximately ± 0.1 and varied along the jets. Several experiments on turbulent boundary layers along convex and concave walls have reported[5,8,9] that the ratio of boundary layer thickness to the radius of curvature of the wall (δ/R) varied from 0.01 to 0.1. It has been reported that the effect of curvature is very large even for a mild curvature $\delta/R \simeq 0.01$. Hence it could have been expected that the present study would show the strong effects of curvature on the turbulence properties.

4-2. Turbulence intensities

Besides the effects of the streamline curvature, the effects of the coflowing ambient, namely the s-component edge velocity U_e in the outer edge, will also be important. Studies on the effects of the coflowing ambient[6] for $U_e/(U_m - U_e) < 0.1$ with a constant edge velocity have shown significant effects. However, in the present study $U_e/(U_m - U_e)$ is at most 0.6 and the edge velocity U_e varies rapidly. Hence the turbulence properties in the outer portion are expected to show strong

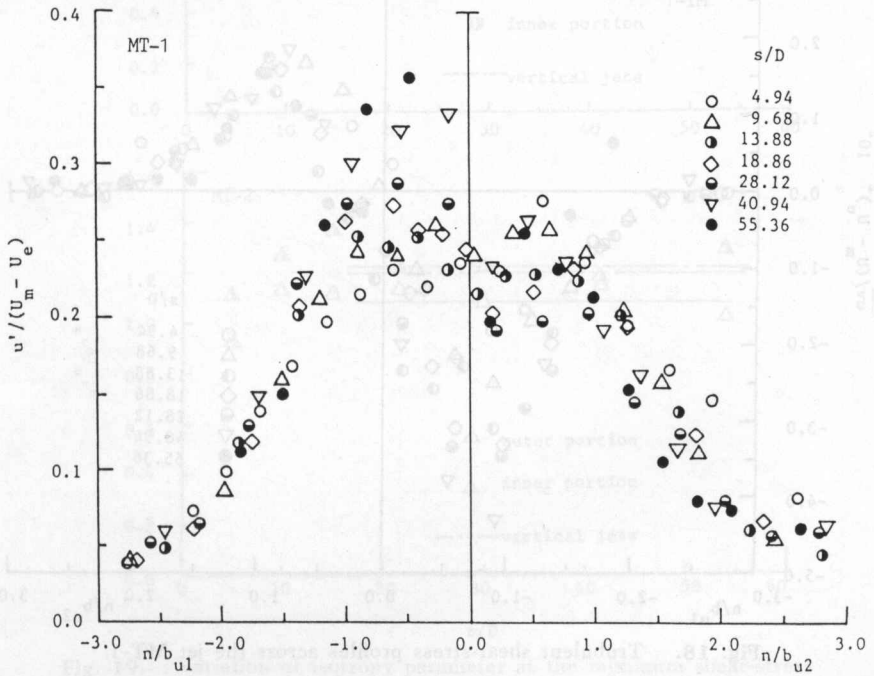

Fig. 16. s-component turbulence intensity profiles across the jet MT-1.

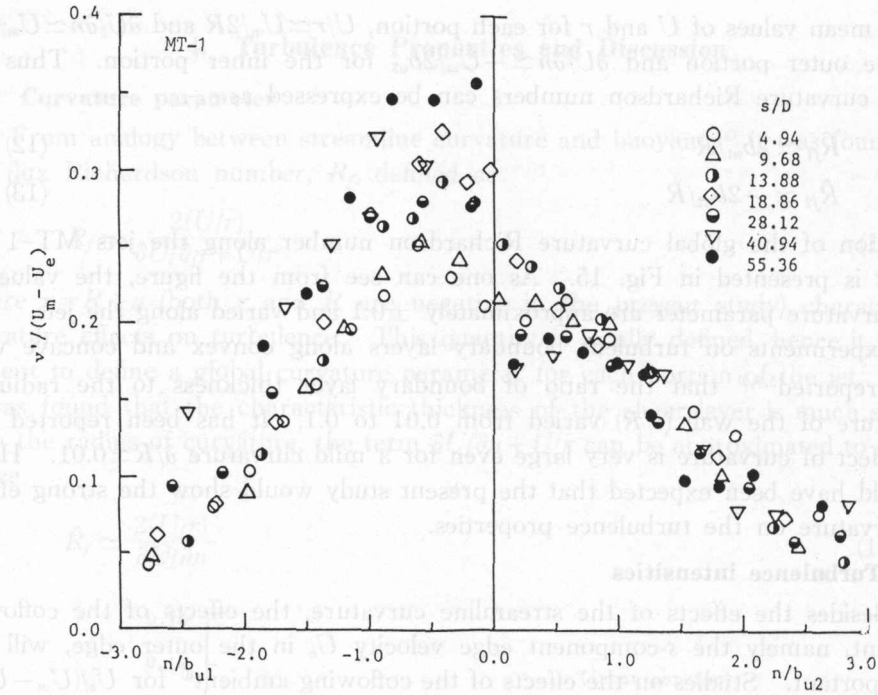

Fig. 17. *n*-component turbulence intensity profiles across the jet MT-1.

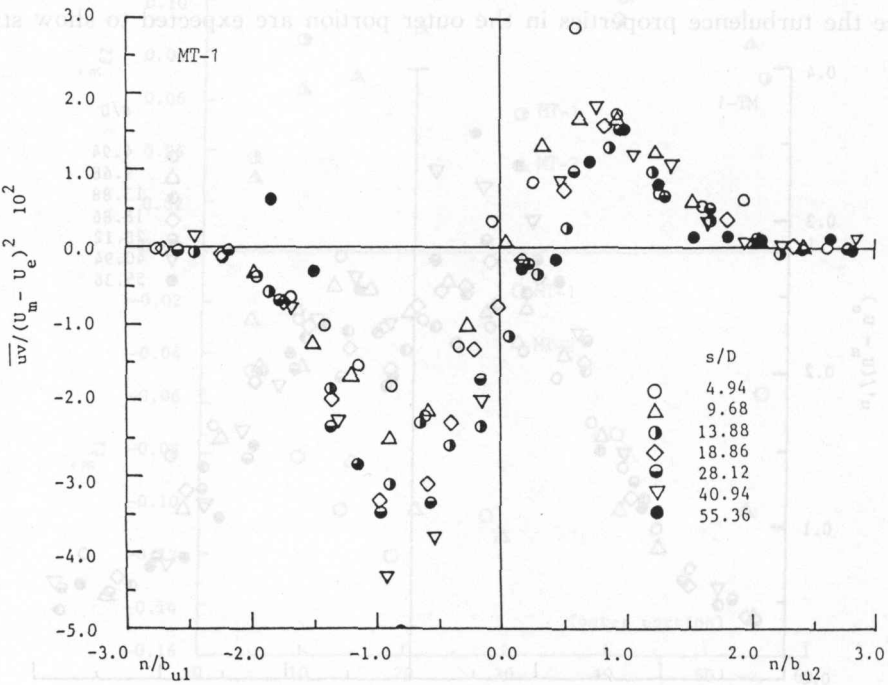

Fig. 18. Trubulent shear-stress profiles across the jet MT-1.

nonequilibrium, while the inner portion should be less subjected to nonequilibrium. Instead of being normalized with U_m and b_u, s- and n-component turbulence intensities u' and v' are normalized with (U_m-U_{e1}) and b_{u1} for the outer portion, while (U_m-U_{e2}) and b_{u2} is used for the inner portion since (U_m-U_e) is the logical velocity scale for a jet in an ambient moving at constant velocity U_e in s-direction.

The s- and n-component turbulence intensities for the jet MT-1 are presented in Fig. 16 and 17. Similar, but less dramatic, results were obtained for the jet MT-2. In the outer portion ($n<0$), evolving trends mostly due to the strong nonequilibrium can be observed. Since, in general, the maximum values of the s- and the n-component normalized turbulence intensities in vertical jets in still ambient are about 0.25 and 0.2 respectively, the appearance of enhancement of turbulence in the outer portion and no significant reduction in the inner portion can be observed.

Profiles of the turbulent shear-stress of the jet MT-1 are presented in Fig.

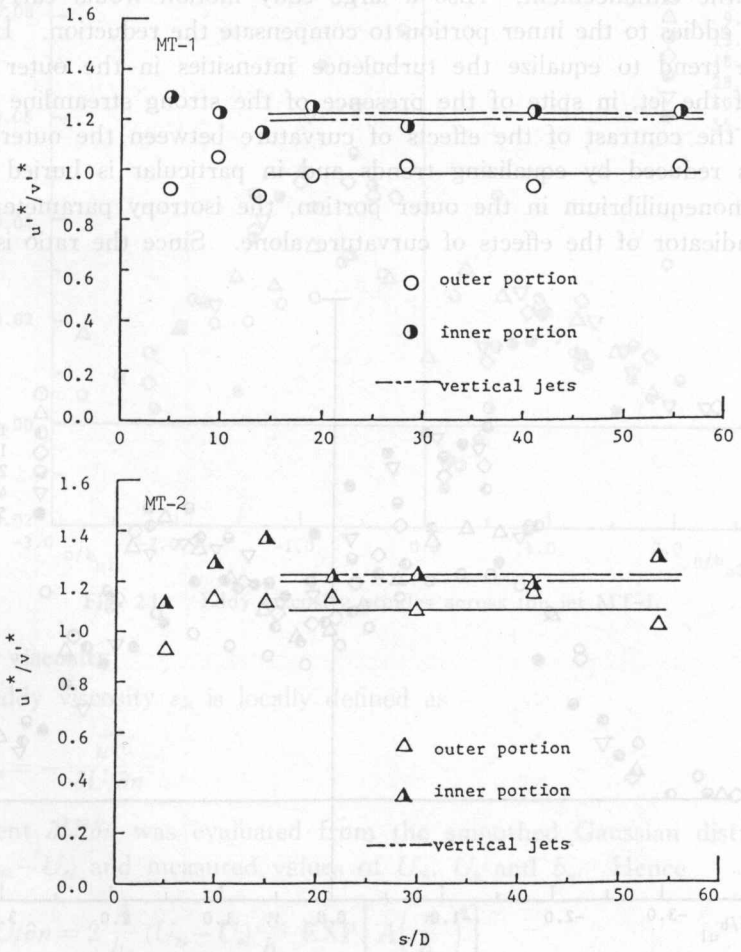

Fig. 19. Variation of isotropy parameter at the miximum shear-stress point along the jets MT-1 and MT-2.

18. Since the normalized maximum shear-stress for a vertical jet is approximately 0.022, enhancement of the shear-stress in the outer portion and slight reduction in the inner portion can be observed. It is also seen from the figure that the location of zero shear-stress does not coincide with the center of the jet, but shifts slightly towards the inner portion of the jet. From the observations of s- and n-component turbilence intensities and the turbulent shear-stress in the inner portion of the jet, it can be considered that there are no such significant effects of curvature as observed in a boundary layer along a convex wall. The same consideration can be applied to the outer portion also, and hence the observed enhancement in the outer portion can be largely due to the nonequilibrium arising from the rapid variation of the s-component edge velocity. As mentioned before, there is a flow passing through the jet centerline from the inner portion to the outer portion to compoensate uneven entrainment between the outer and inner portions. This flow would carry reduced turbulence eddies to the outer portion to reduce the enhancement. Also a large eddy motion would carry enhanced turbulence eddies to the inner portion to compensate the reduction. Hence there must be a trend to equalize the turbulence intensities in the outer and inner portions of the jet, in spite of the presence of the strong streamline curvature.

Since the contrast of the effects of curvature between the outer and inner portions is reduced by equalizing trends and in particular is buried under the effects of nonequilibrium in the outer portion, the isotropy parameter u'/v' can be good indicator of the effects of curvature alone. Since the ratio is independ-

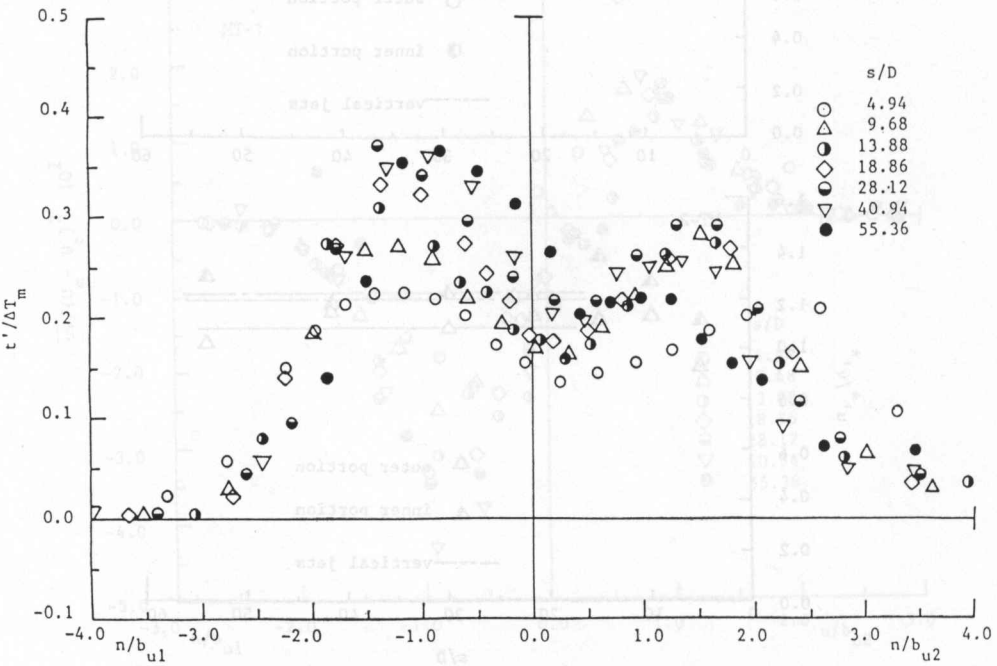

Fig. 20. Profiles of rms intensities of temperature fluctuations across the jet MT-1.

ent of the scaling velocity, this should not be very sensitive to the effects of nonequilibrium, even though u' and v' are individually affected. The values of the isotropy parameter u'/v' at the maximum shear-stress points along each portion of the jet are presented in Fig. 19. As one can see from the figure, clear reduction of n-component turbulence intendities in the inner portion and enhancement in the outer portion can be observed.

Another good indicator of the effects of curvature is the rms intensities of the temperature fluctuations, since the temperature field does not exhibit non-equilibrium in the present study. Fig. 20 shows the distributions of the intensities of temperature fluctuations in the jet MT-1. This shows enhanced turbulence in the outer portion and reduced trubulence in the inner portion.

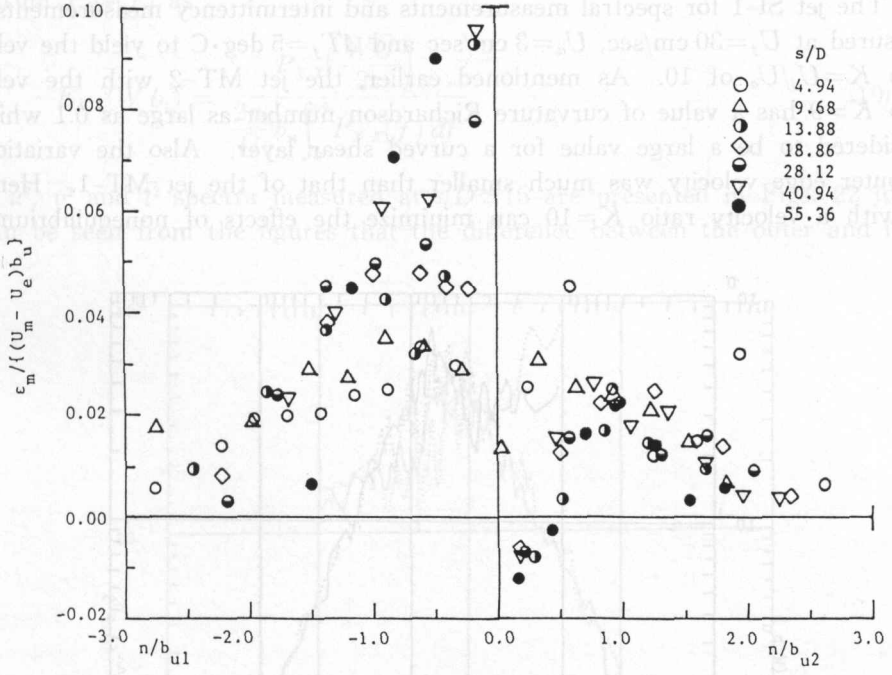

Fig. 21. Eddy viscosity profiles across the jet MT-1.

4-3. Eddy viscosity

The eddy viscosity ε_m is locally defined as

$$\varepsilon_m = -\frac{\overline{uv}}{\partial U/\partial n} \tag{14}$$

The gradient $\partial U/\partial n$ was evaluated from the smoothed Gaussian distribution of $(U-U_e)/(U_m-U_e)$ and measured values of U_m, U_e and b_u. Hence

$$\partial U/\partial n = 2\frac{A}{b_u}(U_m-U_e)\frac{n}{b_u}\,\mathrm{EXP}\left[A\left(\frac{n}{b_u}\right)^2\right] \tag{15}$$

where $A=\ln(0.5)$. Hence the nondimensional eddy viscosity $\hat{\varepsilon}_m$ is calculated as

$$\hat{\varepsilon}_m = \frac{\varepsilon_m}{(U_m - U_e)\, b_u} = \frac{-\overline{uv}/(U_m - U_e)^2}{2A\dfrac{n}{b_u}\,\mathrm{EXP}\left[A\left(\dfrac{n}{b_u}\right)^2\right]} \tag{16}$$

Results for the jet MT-1 are presented in Fig. 21, and similar results were obtained for the jet MT-2. The values for $\hat{\varepsilon}_m$ of a vertical jet are usually considered to be nearly constant across the jet[3]. In the present study, as one can see from the figure, the eddy viscosity varies significantly across the jet. This is mainly due to the fact that the zero shear-stress points do not coincide with the center of the jet. Hence the assumption of constant eddy viscosity across the jet can not be applied to a jet with streamline curvature.

4-4. Spectral analysis

The jet SI-1 for spectral measurements and intermittency measurements was measured at $U_j = 30$ cm/sec, $U_a = 3$ cm/sec and $\Delta T_j = 5$ deg·C to yield the velocity retio $K = U_j/U_a$ of 10. As mentioned earlier, the jet MT-2 with the velocity retio $K = 9$ has a value of curvature Richardson number as large as 0.1 which is considered to be a large value for a curved shear layer. Also the variation of its outer edge velocity was much smaller than that of the jet MT-1. Hence a jet with a velocity ratio $K = 10$ can minimize the effects of nonequilibrium yet

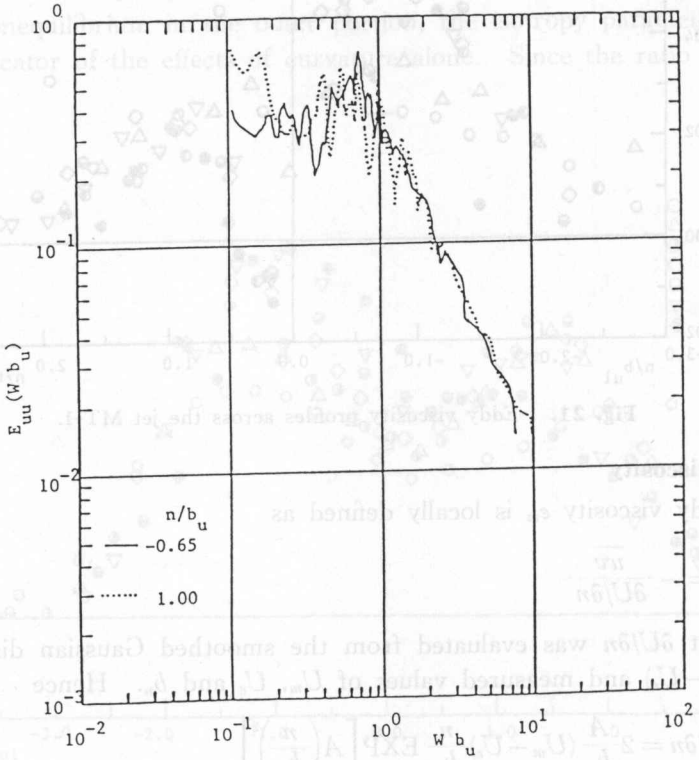

Fig. 22. Comparison of *s*-component spectra between the outer and inner portions of the jet SI-1.

shows identifiable effects of curvature.

In each portion of the jet, spectra were obtained in the vicinity of the maximum shear-stress point. Each spectrum is presented in the wave number domain and the spectral function is normalized such that

$$\int_0^\infty E_{X,X}(W b_u)\, d(W b_u) = 1 \tag{17}$$

where X is the time series u, v or t and W is the wave number defined as

$$W = 2\pi f/\bar{U} \tag{18}$$

with $\bar{U}$ being the mean s-component velocity at the measuring point. Hence the normalized spectral function $E_{X,X}(W b_u)$ is obtained from measured frequency spectrum $P_{X,X}(f)$ as

$$E_{X,X}(W b_u) = \frac{P_{X,X}\left(\dfrac{W\bar{U}}{2\pi}\right)}{\dfrac{2\pi}{\bar{U}} b_u \displaystyle\int_0^\infty P_{X,X}(f)\, df} \tag{19}$$

The $\overline{u^2}$, $\overline{v^2}$ and $\overline{t^2}$ spectra measured at $s/D \simeq 15$ are presented in Figs. 22 to 24. It can be seen from the figures that the difference between the outer and inner

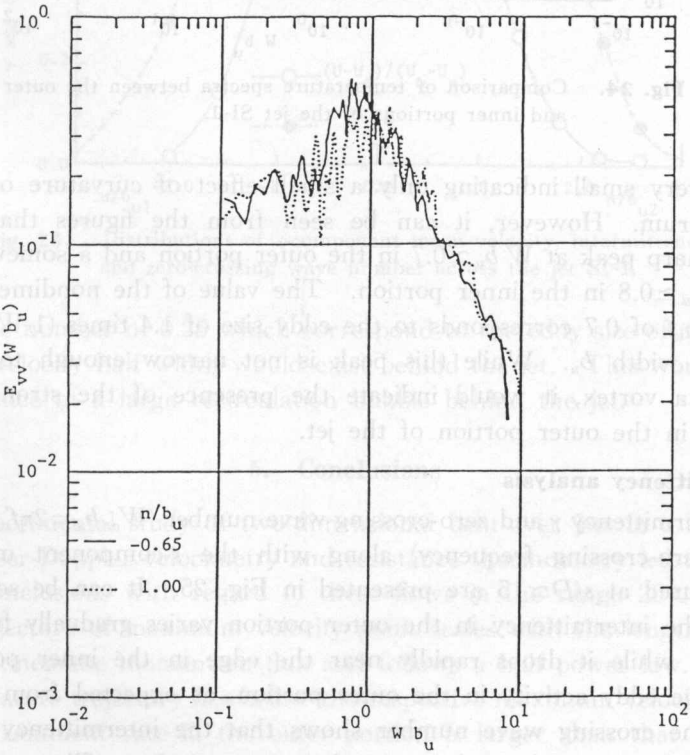

Fig. 23. Comparison of n-component spectra between the outer and inner portions of the jet SI-1.

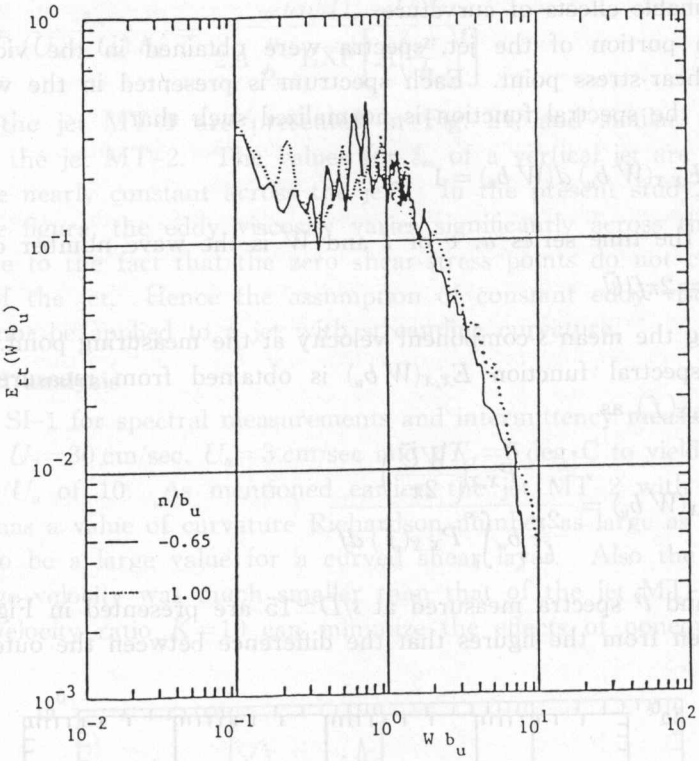

Fig. 24. Comparison of temperature spectra between the outer and inner portions of the jet SI-1.

portions is very small indicating only a small effect of curvature on this range of the spectrum. However, it can be seen from the figures that there is a distinctive sharp peak at $W\,b_u \simeq 0.7$ in the outer portion and a somewhat broader peak at $W\,b_u \simeq 0.8$ in the inner portion. The value of the nondimensional wave number ($W\,b_u$) of 0.7 corresponds to the eddy size of 1.4 times ($1/W = b_u/0.7$) the velocity half width b_u. While this peak is not narrow enough to suggest the presence of a vortex, it would indicate the presence of the strong activity of large eddies in the outer portion of the jet.

4-5. Intermittency analysis

The intermittency γ and zero-crossing wave number ($W_{cr}\,b_u = 2\pi f_{cr}\,b_u/\bar{U}$, where f_{cr} is the zero-crossing frequency) along with the s-component mean velocity profile measured at $s/D \simeq 15$ are presented in Fig. 25. It can be seen from the figure that the intermittency in the outer portion varies gradually from the axis to the edge, while it drops rapidly near the edge in the inner portion. This indicates large eddy activity in the outer portion, as expected from the spectral analysis. The crossing wave number shows that the intermittency is produced by eddies of wave number of 0.8 in the outer portion. These eddies would correspond to the peak in the energy spectra. In the inner portion eddies of the

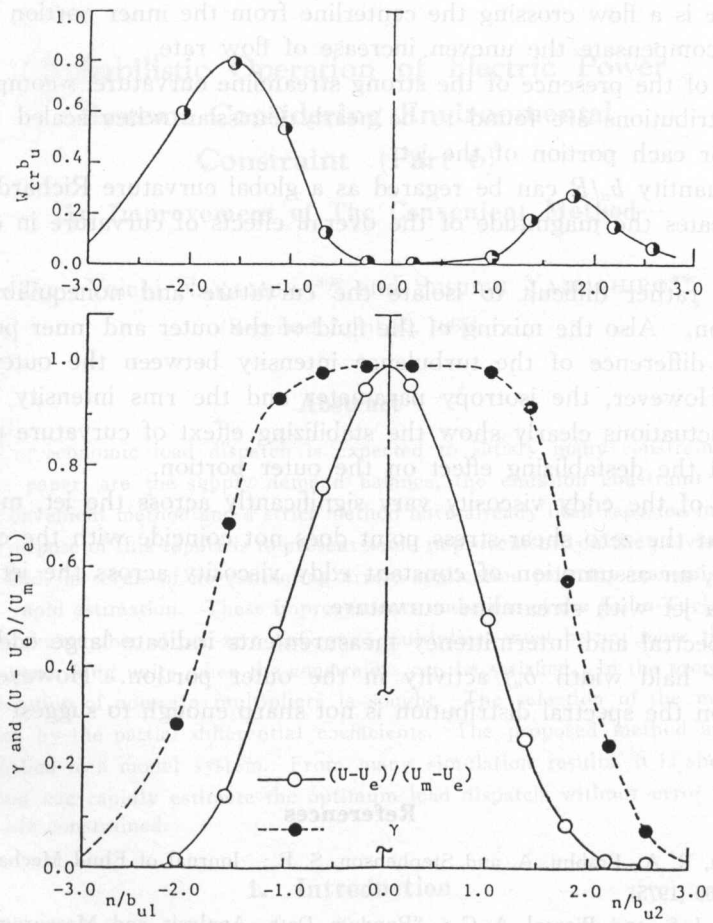

Fig. 25. Distributions of s-component mean velocity, intermittency and zero-crossing wave number across the jet SI-1.

crossing wave number of 0.25 which correspond to the eddy size of approximately 4 times the velocity half width would exist behind the jet. This would be caused by the presence of a large recirculation bubble behind the jet.

5. Conclusions

The experimental study of two-dimensional bent-over jets in a cross-flow by means of Laser-Doppler velocimetry and resistance thermometry led to the following major conclusions with regard to these flows in the range $20<s/D<60$.

1. The trajectory of maximum velocity point scales with the length scale based on the exit kinematic momentum flux and follows a half power law. The maximum temperature trajectory lies below the respective maximum velocity trajectory.

2. The entrainment rate in the outer portion is larger than that of a vertical jet due to the presence of the significant positive s-component edge velocity at the outer edge, while the inner portion does not show significant difference.

Hence there is a flow crossing the centerline from the inner portion to the outer portion to compensate the uneven increase of flow rate.

3. Inspite of the presence of the strong streamline curvature, s-component mean velocity distributions are found to be nearly Gaussian when scaled with b_u and $(U_m - U_e)$ for each portion of the jet.

4. The quantity b_u/R can be regared as a global curvature Richardson number which indicates the magnitude of the overall effects of curvature in each portion of the jet.

5. It was rather difficult to isolate the curvature and nonequilibrium in the outer portion. Also the mixing of the fluid of the outer and inner portion would reduce the difference of the turbulence intensity between the outer and inner portions. However, the isotropy parameter and the rms intensity of the temperature fluctuations clearly show the stabilizing effext of curvature on the inner portion and the destablizing effect on the outer portion.

6. Values of the eddy viscosity vary significantly across the jet, mainly due to the fact that the zero shear-stress point does not coincide with the center of the jet. Hence, an assumption of constant eddy viscosity across the jet can not be applied to a jet with streamline curvature.

7. The spectral and intermittency measurements indicate large eddy (1.4 times the velocity hald width b_u) activity in the outer portion. However, the peak appearing on the spectral distribution is not sharp enough to suggest the presence of a vortex.

References

1) Antonia, R. A., Prabhu, A. and Stephenson, S. E.: Journal of Fluid Mechanics, Vol. 72, p. 455 (1975).
2) Bendat, J. S. and Piersol, A. G.: "Random Data, Analysis and Measurement", Wiley-Interscience, New York (1971).
3) Bradbury, L. J. S.: Journal of Fluid Mechanics, Vol. 23, p. 31 (1965).
4) Bradshaw, P.: Journal of Fluid Mechanics, Vol. 36, p. 177 (1969).
5) Ellis, L. B. and Joubert, P. N.: Journal of Fluid Mechanics, Vol. 62, p. 65 (1974).
6) Everitt, W. K. and Robins, G. A.: Journal of Fluid Mechanics, Vol. 88 p. 563 (1978).
7) LaRue, J. C.: Physics of Fluids, Vol. 17, No. 8, p. 1513 (August 1974).
8) Ramaprian, B. R. and Shivaprasad, B. G.: Journal of Fluid Mechanics, Vol. 85, Part 2, p. 273 (1978).
9) So, R. M. C. and Millor, G. L.: Journal of Fluid Mechanics, Vol. 60, p. 43 (1973).
10) Webster, C. A. G.: Journal of Fluid Mechanics, Vol. 19, p. 221 (1964).
11) Weir, A. D., Wood, D. H. and Bradshaw, P.: Journal of Fluid Mechanics, Vol. 107, p. 237 (1981).